JOURNAL OF SPACECRAFT AND ROCKETS
Vol. 33, No. 6, November–December 1996

Deployment and Retraction of a Cable-Driven Rigid Panel Solar Array

P. Kumar* and S. Pellegrino†
University of Cambridge, Cambridge CB2 1PZ, England, United Kingdom

Cable-driven rigid panel solar arrays are deployed and retracted by two or more continuous cables running over free-turning pulleys. Each cable is connected to a motorized drum, and synchronization between the panels is maintained by a series of cable loops. Experiments on a small-scale model array show that the distribution of forces in the elements of the array varies during deployment and retraction because of an interaction between geometry change effects and joint friction. A quasistatic analytical model of the deployment/retraction process is presented, which is able to predict the main features of the behavior observed in the experiments. The interaction forces between the model array and the gravity compensation system are measured during the tests and are also included in the simulation.

Introduction

THIS paper investigates the deployment and retraction behavior of rigid panel solar arrays, often used for low-Earth-orbit missions. Usually, arrays of this type are deployed by torsion springs[1–4] and hence cannot be retracted. Cable-driven arrays are used when a retraction capability is required as, for example, in the European retrievable carrier (EURECA). Typically, two or more continuous cables run over a series of free turning pulleys connected to the hinges of the array, and one end of each cable is connected to a motorized drum. A series of cable loops removes all remaining kinematic freedoms from the system.

Figure 1 shows schematically an array consisting of a yoke (1_2) and five panels (2_3, 3_4, etc.); this is the particular layout that will be investigated in this paper. A general configuration of the array is defined by the angle α. During deployment α increases from approximately 0 deg, in the folded configuration, to approximately 90 deg in the deployed configuration. Deployment of the array is activated by shortening the length of deployment cable (Fig. 1b) by turning the deployment cable drum in a clockwise sense. The array is retracted by shortening the retraction cable (Fig. 1c), i.e., by turning the retraction cable drum in an anticlockwise sense. Of course, during deployment the retraction cable must also be lengthened, by turning its drum in a clockwise sense, whereas during retraction the deployment cable must be lengthened. Because only the length of cable wound over the pulleys can vary, the total length of cable that is wound/unwound during deployment/retraction is quite small. Note that no hinge latches are used in this type of array. Instead, at the end of deployment the hinges are preloaded by pretensioning the deployment cable. For redundancy, and also to avoid torsional deformation of the array, it is common to use two deployment cables, one on each side of the array, and two retraction cables.

The deployment and retraction cables control only one of the six degrees of freedom (DOF) of the array. The five DOF that are left are eliminated by introducing five closed contact loops (CCL). Each CCL is mounted alongside a panel and looped over pulleys that are free to rotate with respect to that panel, but are fixed to the adjacent panels. For example, in the CCL shown in Fig. 1d the pulley at hinge 3 is fixed to panel 2_3, whereas the pulley at hinge 4 is fixed to panel 4_5. Provided that this CCL does not slip over the two pulleys, panels 2_3 and 4_5 will remain parallel.

To guarantee the correct deployment/retraction of such an array in the space environment, accurate predictions of the distribution of forces in the elements of the array are required. These forces vary during deployment, because of a complex interaction between geometry change effects and friction torques. This paper presents an analytical model of the deployment process whose predictions are compared to the actual behavior of a small-scale model array. The effects of the gravity compensation system on the behavior of the model array are included in the analytical model.

Model Array

A small-scale model array, loosely based on the retractable advanced rigid array[5,6] used in the EURECA spacecraft, is shown in Fig. 2. This model is approximately 2.3 m long (fully deployed) and 0.3 m wide. It consists of one half-length panel, functionally equivalent to the yoke, and five full-length panels (length L = 0.4 m

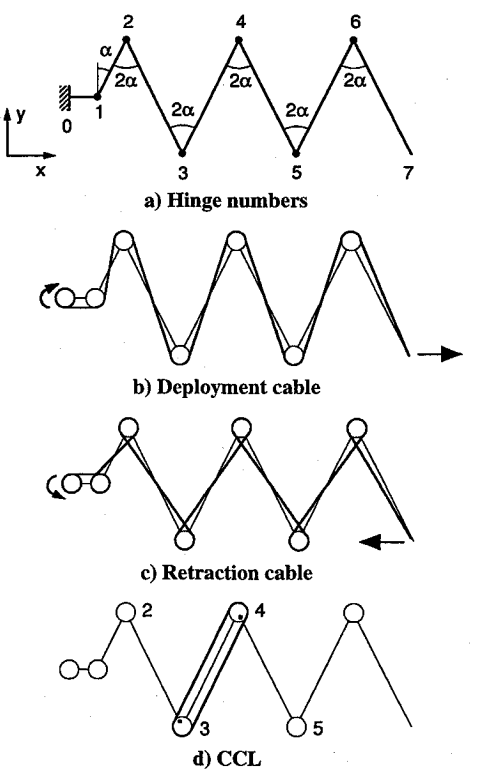

Fig. 1 Operating principle of cable-driven arrays.

Presented as Paper 95-1367 at the AIAA/ASME/ASCE/AHS/ASC 36th Structures, Structural Dynamics, and Materials Conference, New Orleans, LA, April 10–13, 1995; received July 7, 1995; revision received Feb. 5, 1996; accepted for publication March 8, 1996.

*Research Student, Department of Engineering, Trumpington Street. Student Member AIAA.

†Lecturer, Department of Engineering, Trumpington Street. Member AIAA.

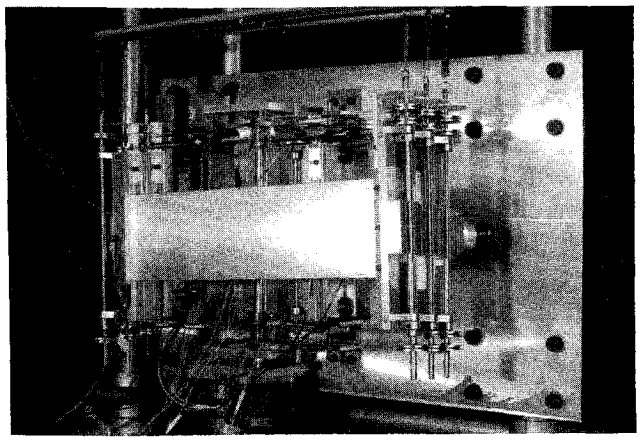

a) Folded

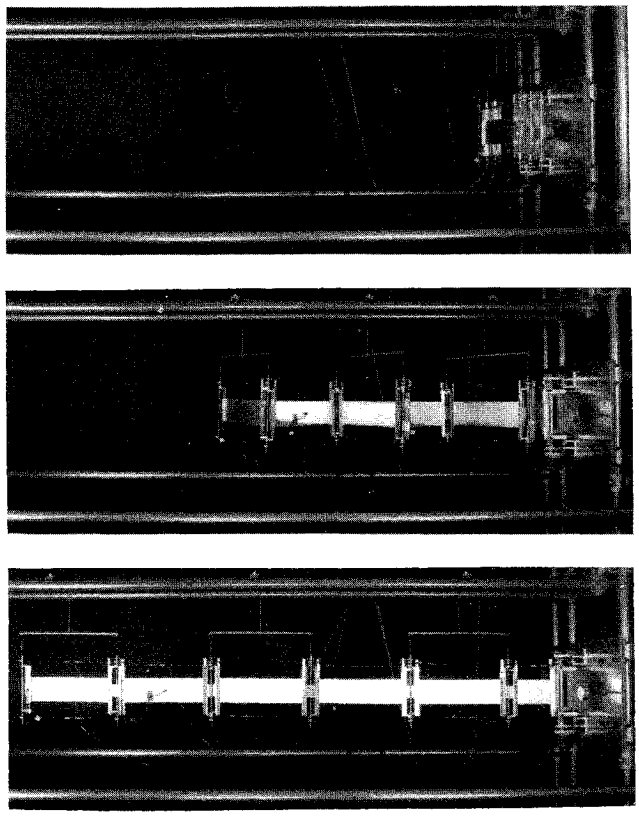

b) During deployment

Fig. 2 Model array.

between hinge centers). The panels are 1.6-mm-thick Al-alloy plates, connected by Al-alloy hinge assemblies through continuous stainless steel shafts (radius $s = 3$ mm).

The deployment and retraction cables (multistranded steel cables with diameter 0.8 mm) are mounted one on each side of the array. These cables run over free turning pulleys (radius $p = 12.5$ mm), which are mounted on the hinge shafts, and are connected at one end to coaxially mounted Al-alloy drums, driven by a single stepper motor. The panels are synchronized by five prestressed CCLs, each consisting of a multistranded steel cable in series with a steel spring (pretension $T = 30$ N) and looped over pulleys that are also mounted on the hinge shafts. Each pulley is fixed to one side of the hinge assembly, as explained in the Introduction. All contact surfaces are PTFE (polytetrafluoroethylene) lined journal bearings (friction coefficient $\mu = 0.15$). The array is deployed horizontally and its weight is off loaded through three pairs of strain-gauged support elements connected to independent linear bearings running on horizontal rails (see Fig. 2b). The total mass of the moving parts is 4.7 kg. The cable tensions in the array are monitored by strain-gauged elements mounted on the deployment and the retraction cables, whereas the torques applied by the CCL's looped around panels 2_3 and 5_6 are measured by pairs of strain-gauged elements. Further details on this experiment are given in Ref. 7.

Deployment and Retraction Experiments

All experiments have been carried out over 60 s, with the motor turning at a constant rate. Figures 3a, 3b, 4a, and 4b show the tension variation in the deployment and retraction cables during such an experiment. Their values are denoted by $D_{i\_(i+1)}$ and $R_{i\_(i+1)}$, respectively, for a measurement point lying between hinges i and $(i + 1)$. The coupling torques applied by the CCLs looped around panels 2_3 and 5_6 are shown in Figs. 3c and 4c; $C_{i\_(i+1)}$ is defined positive if it acts in a clockwise direction on panel $(i + 1)\_(i + 2)$. The forces applied to each hinge shaft by the gravity compensation system are plotted in Figs. 3d and 4d.

Results from a particular deployment test are shown in Fig. 3. At the start, the deployment cable is almost slack, $D_{2\_3} \cong D_{6\_7} \cong 2$ N (Fig. 3a), but the retraction cable is pretensioned to $R_{2\_3} \cong R_{6\_7} \cong 30$ N (Fig. 3b). As the array starts to deploy, the deployment cable tensions increase up to $D_{2\_3} \cong 7$ N, $D_{6\_7} = 4$ N and then

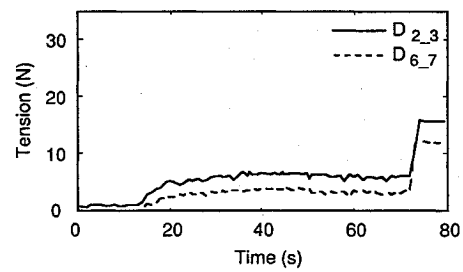

a) Deployment cable tensions

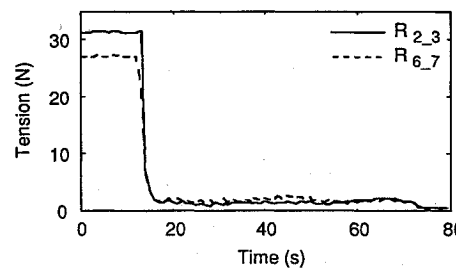

b) Retraction cable tensions

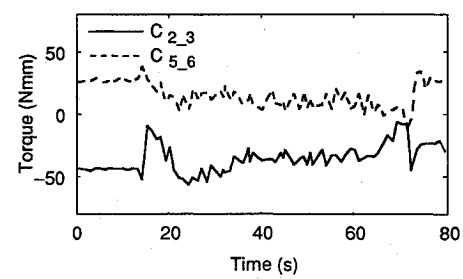

c) CCL torques

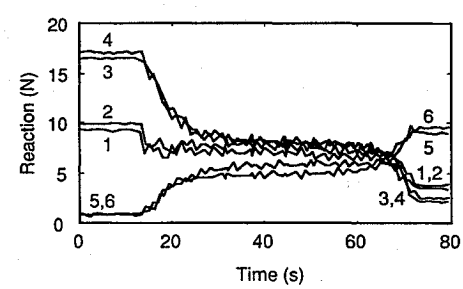

d) Compensation system reactions

Fig. 3 Measured deployment behavior.

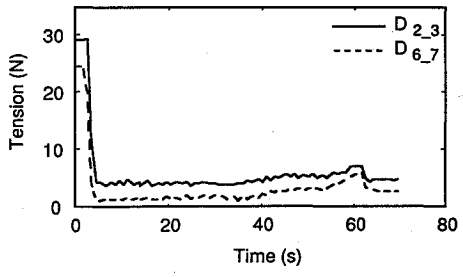

a) Deployment cable tensions

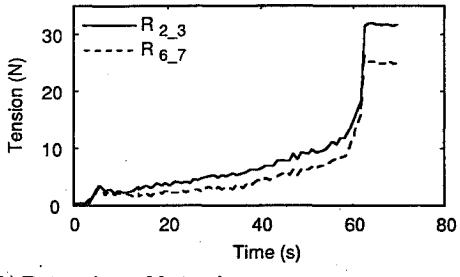

b) Retraction cable tensions

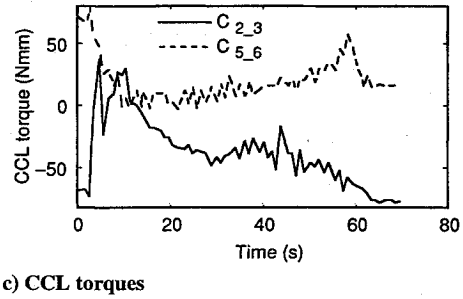

c) CCL torques

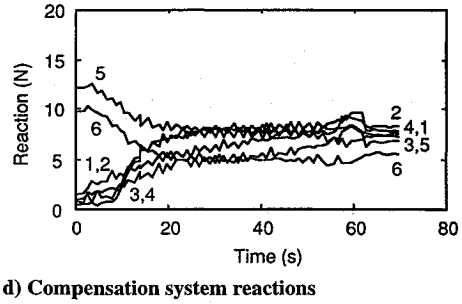

d) Compensation system reactions

Fig. 4 Retraction behavior.

start decreasing. The retraction cable tensions quickly decrease to $D_{2\_3} \cong D_{6\_7} \cong 2$ N and then remain approximately constant. When the array is about to reach its fully deployed shape, the tension in the deployment cable quickly increases until the motor is stopped. The two CCL torques show initial sharp variations followed by slow increases in magnitude, with $C_{2\_3} < 0$ and $C_{5\_6} > 0$. The magnitude of these torques is quite small and, since the change of tension in the CCLs is less than 2 N, the noise level in these measurements is quite high. The forces applied by the gravity compensation system (Fig. 3d) are evenly distributed when the array is approximately half-deployed, but are very uneven at the start and at the end of the process. Also, their distributions are quite different for $\alpha = 0$ and 90 deg.

Corresponding results from a retraction test are shown in Figs. 4a–4d. At the start, corresponding to the end of a deployment test in Fig. 3, the retraction cable is slack and the deployment cable is prestressed. As the array is retracted, the tensions in the retraction cable steadily increase from about 4 N to about 10 N, whereas the tensions in the deployment cable show a sudden drop at the start, followed by a slow rise. The CCL torques vary over a wider range than in the deployment test.

Analytical Model of Deployment

The root element 0_1, the yoke 1_2, and the five panels of the array can be modeled, in two dimensions, as a concertina of seven beams connected by hinges (Fig. 1a). The beams are constrained by five CCL elements and by the deployment and retraction cables (not shown in the figure). The whole assembly is rigidly supported at the root. During deployment the tensions in the retraction cable are known, whereas the tensions in the deployment cable can be expressed in terms of a single unknown value.

The deployment process can be modeled by a system of equilibrium equations relating a set of internal variables to a set of external variables. The internal variables include the axial force, shear force, and bending moment at a section of each beam, as well as the couple transmitted by each CCL and the tension at a chosen section of the deployment cable. The external variables are the 2 components of external force at each hinge, applied by the retraction cable, and the 2 external couples on either side of that hinge, applied by the hinge shaft. Therefore, the total number of internal variables is equal to three times the number of beams, plus the number of CCLs, plus 1, i.e., 27. The total number of external variables is also 27, since there are two force components and two couples at hinges 1–6 but only two force components and a couple at hinge 7. For any chosen configuration of the array, a system of 27 equations in 27 unknowns can be set up from the equilibrium equations of each element.

Beams

Figure 5 shows the beam element linking hinges i to $i+1$. Taking as internal variables the axial force $t_{i\_(i+1)}$, shear force $q_{i\_(i+1)}$, and bending moment $m_{i\_(i+1)}$ near hinge $(i + 1)$, and using the sign convention shown in Fig. 5, the external and internal variables are related by a set of six equilibrium equations, whose matrix form is

$$\begin{bmatrix} \boldsymbol{A}_{i\_(i+1)} \\ \boldsymbol{B}_{i\_(i+1)} \\ -\boldsymbol{A}_{i\_(i+1)} \\ \boldsymbol{C}_{i\_(i+1)} \end{bmatrix} \begin{bmatrix} t_{i\_(i+1)} \\ q_{i\_(i+1)} \\ m_{i\_(i+1)} \end{bmatrix} = \begin{bmatrix} f_{ix} \\ f_{iy} \\ g_{i\_(i+1)} \\ f_{(i+1)x} \\ f_{(i+1)y} \\ g_{(i+1)\_i} \end{bmatrix} \tag{1}$$

where

$$\boldsymbol{A}_{i\_(i+1)} = \begin{bmatrix} -\cos\beta_{i\_(i+1)} & \sin\beta_{i\_(i+1)} & 0 \\ -\sin\beta_{i\_(i+1)} & -\cos\beta_{i\_(i+1)} & 0 \end{bmatrix}$$

$$\boldsymbol{B}_{i\_(i+1)} = \begin{bmatrix} 0 & -L_{i\_(i+1)} & -1 \end{bmatrix}$$

$$\boldsymbol{C}_{i\_(i+1)} = [0 \quad 0 \quad 1]$$

Deployment Cable

Consider the pulley that supports the deployment cable at hinge i. This pulley, shown in Fig. 6, is subject to the forces $D_{(i-1)\_i}$ and

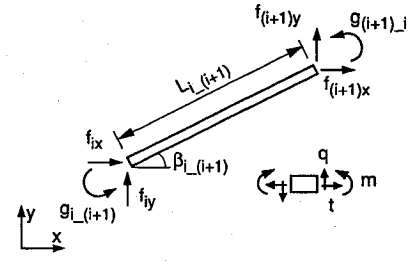

Fig. 5 Beam element.

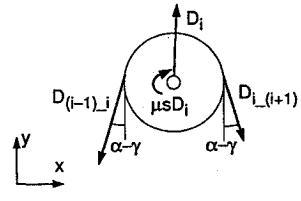

Fig. 6 Deployment cable pulley.

$D_{i\_(i+1)}$, applied by the deployment cable, to a force D_i applied by the hinge shaft, and to a friction couple of magnitude $\mu s D_i$. At most hinges the deployment cable forces form an angle of magnitude $\alpha - \gamma$ with the y axis, where

$$\gamma = \arctan(2p/L) \tag{2}$$

For equilibrium in the x and y directions

$$\begin{aligned} D_{ix} &= \left(D_{(i-1)\_i} - D_{i\_(i+1)}\right)\sin(\alpha-\gamma) \\ D_{iy} &= \left(D_{(i-1)\_i} + D_{i\_(i+1)}\right)\cos(\alpha-\gamma) \end{aligned} \tag{3}$$

and, taking moments about the center of the shaft,

$$\left(D_{(i-1)\_i} - D_{i\_(i+1)}\right)p = \mu s D_i \tag{4}$$

Then, substituting $D_i = \sqrt{(D_{ix}^2 + D_{iy}^2)}$ into Eq. (4), expressing D_{ix} and D_{iy} by means of Eq. (3), and rearranging gives

$$d^2 - 2\frac{1+\mu^{*2}\cos 2(\alpha-\gamma)}{1-\mu^{*2}}d + 1 = 0 \tag{5}$$

where d is the standard ratio of the cable tensions on either side of the pulley:

$$d = \frac{D_{(i-1)\_i}}{D_{i\_(i+1)}} \tag{6}$$

and

$$\mu^* = \mu s/p \tag{7}$$

Of the two solutions of this quadratic equation, only $d \geq 1$ is of interest; hence,

$$d = \frac{1}{1-\mu^{*2}}\Big\{1 + \mu^{*2}\cos 2(\alpha-\gamma) + \mu^*\sqrt{2 + 2\cos 2(\alpha-\gamma) + \mu^{*2}[\cos^2 2(\alpha-\gamma) - 1]}\Big\} \tag{8}$$

The preceding analysis is not valid for pulley 1, where D_{0_1} is parallel to the x axis and D_{1_2} forms an angle $\alpha - \gamma_1$ with the y axis, where

$$\gamma_1 = \arctan(4p/L) \tag{9}$$

By an analysis similar to that already described, it is found that

$$d_1 = \frac{D_{0\_1}}{D_{1\_2}} = \frac{1}{1-\mu^{*2}}\Big[1 - \mu^{*2}\sin(\alpha-\gamma_1) + \mu^*\sqrt{2 - 2\sin(\alpha-\gamma_1) - \mu^{*2}\cos^2(\alpha-\gamma_1)}\Big] \tag{10}$$

A similar problem arises at pulley 2 but, since the components of the deployment cable forces are approximately equal to those given in Eq. (3), the standard ratio d will be assumed for all pulleys other than 1. Also, pulley 6 does not turn relative to panel 6_7; hence it will be assumed that $D_{5\_6} = D_{6\_7}$.

With the preceding relationships, all deployment cable tensions can be expressed in terms of D_{0_1}, as follows:

$$D_{1\_2} = D_{0\_1}/d_1;\ D_{2\_3} \cong D_{0\_1}/d_1 d;\ \ldots;\ d_{5\_6} = D_{6\_7} = D_{0\_1}/d_1 d^4 \tag{11}$$

The shaft that supports pulley i applies to the hinge a force equal and opposite to D_i. Therefore, expressing $D_{(i-1)\_i}$ and $D_{i\_(i+1)}$ in Eq. (3) in terms of D_{0_1}, two equilibrium equations are obtained:

$$\boldsymbol{E}_i[D_{0\_1}] = \begin{bmatrix} f_{ix} \\ f_{iy} \end{bmatrix} \tag{12}$$

where

$$\boldsymbol{E}_1 = \begin{bmatrix} 1 - \dfrac{\sin(\alpha-\gamma_1)}{d_1} \\ -\dfrac{\cos(\alpha-\gamma_1)}{d_1} \end{bmatrix}$$

$$\boldsymbol{E}_2 = \begin{bmatrix} \dfrac{\sin(\alpha-\gamma_1)}{d_1} - \dfrac{\sin(\alpha-\gamma)}{d_1 d} \\ \dfrac{\cos(\alpha-\gamma_1)}{d_1} + \dfrac{\cos(\alpha-\gamma)}{d_1 d} \end{bmatrix}$$

$$\boldsymbol{E}_i = \begin{bmatrix} \dfrac{d-1}{d_1 d^{(i-1)}}\sin(\alpha-\gamma) \\ \pm\dfrac{d+1}{d_1 d^{(i-1)}}\cos(\alpha-\gamma) \end{bmatrix} \qquad \begin{cases} +\text{for } i = 4 \\ -\text{for } i = 3, 5 \end{cases}$$

$$\boldsymbol{E}_6 = \begin{bmatrix} \dfrac{\sin(\alpha-\gamma) - \sin(\alpha-\gamma/2)}{d_1 d^4} \\ \dfrac{\cos(\alpha-\gamma) + \cos(\alpha-\gamma/2)}{d_1 d^4} \end{bmatrix}$$

$$\boldsymbol{E}_7 = \begin{bmatrix} \dfrac{\sin(\alpha-\gamma/2)}{d_1 d^4} \\ -\dfrac{\cos(\alpha-\gamma/2)}{d_1 d^4} \end{bmatrix}$$

CCLs

Consider the CCL that loops over hinges i and $i+1$. Initially, it carries a uniform pretension T that induces a compression of magnitude $2T$ in panel $i\_(i+1)$. During deployment, the tension increases on one side of the loop, whereas it decreases by an equal amount on the other side and, thus, the CCL applies equal and opposite couples $C_{i\_(i+1)}$ to panels $(i-1)\_i$ and $(i+1)\_(i+2)$. The sign convention for $C_{i\_(i+1)}$ is defined in the section Deployment and Retraction Experiments.

For moment equilibrium the following set of equilibrium equations has to be satisfied:

$$\begin{bmatrix} +1 \\ -1 \end{bmatrix}\left[C_{i\_(i+1)}\right] = \begin{bmatrix} g_{i\_(i-1)} \\ g_{(i+1)\_(i+2)} \end{bmatrix} \tag{13}$$

Equilibrium Matrix

Figure 7 shows the 27 × 27 equilibrium matrix that relates the internal and external variables. This matrix is formed from Eqs. (1), (12), and (13). Vertical lines identify the 21-column block that corresponds to the 7 beam elements, the 1-column block corresponding to the deployment cable, and the 5-column block corresponding to the 5 CCLs. Horizontal lines separate the equilibrium equations for different hinges.

Load Vector

The load vector on the right-hand side of the system of equilibrium equations shown in Fig. 7 contains the components of the force applied at each hinge by the retraction cable, as well as the couples applied by each shaft.

Given R_{0_1}, one can compute the standard ratio r of the cable tensions on either side of the pulley (Fig. 8):

$$r = \frac{R_{(i-1)\_i}}{R_{i\_(i+1)}} = \frac{1}{1-\mu^{*2}}\Big\{1 + \mu^{*2}\cos 2(\alpha+\gamma) - \mu^*\sqrt{2 + 2\cos 2(\alpha+\gamma) + \mu^{*2}[\cos^2 2(\alpha+\gamma] - 1}\Big\} \tag{14}$$

which for pulley 1 becomes

$$r_1 = \frac{R_{0\_1}}{R_{1\_2}} = \frac{1}{1-\mu^{*2}}\Big[1 - \mu^{*2}\sin(\alpha-\gamma_1) - \mu^*\sqrt{2 - 2\sin(\alpha+\gamma_1) - \mu^{*2}\cos^2(\alpha+\gamma_1)}\Big] \tag{15}$$

$$
\begin{bmatrix}
-A_{0\_1} & A_{1\_2} & & & & & & & E_1 & -1 & & & & & & \\
C_{0\_1} & & & & & & & & & & & & & & & \\
 & B_{1\_2} & & & & & & & & & & & & & & \\
\hline
 & -A_{1\_2} & A_{2\_3} & & & & & & E_2 & & -1 & & & & & \\
 & C_{1\_2} & & & & & & & & & & & & & & \\
 & & B_{2\_3} & & & & & & & & +1 & & & & & \\
\hline
 & & -A_{2\_3} & A_{3\_4} & & & & & E_3 & & & -1 & & & & \\
 & & C_{2\_3} & & & & & & & & & & & & & \\
 & & & B_{3\_4} & & & & & & & +1 & & & & & \\
\hline
 & & & -A_{3\_4} & A_{4\_5} & & & & E_4 & & & & -1 & & & \\
 & & & C_{3\_4} & & & & & & & & & & & & \\
 & & & & B_{4\_5} & & & & & & & +1 & & & & \\
\hline
 & & & & -A_{4\_5} & A_{5\_6} & & & E_5 & & & & & -1 & & \\
 & & & & C_{4\_5} & & & & & & & & & & & \\
 & & & & & B_{5\_6} & & & & & & & +1 & & & \\
\hline
 & & & & & -A_{5\_6} & A_{6\_7} & & E_6 & & & & & & & \\
 & & & & & C_{5\_6} & & & & & & & & & & \\
 & & & & & & B_{6\_7} & & & & & & & +1 & & \\
\hline
 & & & & & & -A_{6\_7} & & E_7 & & & & & & & \\
 & & & & & & C_{6\_7} & & & & & & & & &
\end{bmatrix}
\begin{bmatrix}
t_{0\_1} \\ q_{0\_1} \\ m_{0\_1} \\ t_{1\_2} \\ q_{1\_2} \\ m_{1\_2} \\ t_{2\_3} \\ q_{2\_3} \\ m_{2\_3} \\ t_{3\_4} \\ q_{3\_4} \\ m_{3\_4} \\ t_{4\_5} \\ q_{4\_5} \\ m_{4\_5} \\ t_{5\_6} \\ q_{5\_6} \\ m_{5\_6} \\ t_{6\_7} \\ q_{6\_7} \\ m_{6\_7} \\ \hline D_{0\_1} \\ \hline C_{1\_2} \\ C_{2\_3} \\ C_{3\_4} \\ C_{4\_5} \\ C_{5\_6}
\end{bmatrix}
=
\begin{bmatrix}
f_{1x} \\ f_{1y} \\ g_{1\_0} \\ \underline{g_{1\_2}} \\ \hline f_{2x} \\ f_{2y} \\ g_{2\_1} \\ \underline{g_{2\_3}} \\ \hline f_{3x} \\ f_{3y} \\ g_{3\_2} \\ \underline{g_{3\_4}} \\ \hline f_{4x} \\ f_{4y} \\ g_{4\_3} \\ \underline{g_{4\_5}} \\ \hline f_{5x} \\ f_{5y} \\ g_{5\_4} \\ \underline{g_{5\_6}} \\ \hline f_{6x} \\ f_{6y} \\ g_{6\_5} \\ \underline{g_{6\_7}} \\ \hline f_{7x} \\ f_{7y} \\ g_{7\_6}
\end{bmatrix}
$$

Fig. 7 System of equilibrium equations.

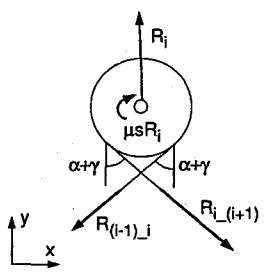

Fig. 8 Retraction cable pulley.

Hence,

$$R_{1\_2} = R_{0\_1}/r_1; \quad R_{2\_3} \cong R_{0\_1}/r_1 r; \ldots; R_{5\_6} = R_{6\_7} = R_{0\_1}/r_1 r^4 \tag{16}$$

In conclusion, the force components applied to hinge i are

$$f_{ix} = -R_{ix} \qquad f_{iy} = -R_{iy} \tag{17}$$

where R_{ix} and R_{iy} are the components of the force R_i applied by the shaft to pulley i. For a standard hinge, in the middle of the array

$$\begin{aligned} R_{ix} &= \left(R_{(i-1)\_i} - R_{i\_(i+1)}\right)\sin(\alpha+\gamma) \\ R_{iy} &= \pm\left(R_{(i-1)\_i} + R_{i\_(i+1)}\right)\cos(\alpha+\gamma) \end{aligned} \qquad \begin{cases} + \text{ for } i = 4 \\ - \text{ for } i = 3, 5 \end{cases} \tag{18}$$

with somewhat different expressions at hinges 1, 2, 6, and 7.

The couples $g_{(i-1)\_i}$ and $g_{i\_(i+1)}$ applied on hinge i are computed by considering the couples acting on the shaft through this hinge, as follows. The shaft of the hinge is subject to a number of forces: D_i and R_i applied by the pulleys that support the deployment and retraction cables, two forces of magnitude $2T$ applied by the pulleys that support the CCLs, and two equal and opposite reaction forces applied by the panels. It is also subject to the forces

$$\begin{aligned} A_{(i-1)\_i} &= \sqrt{t^2_{(i-1)\_i} + q^2_{(i-1)\_i}} \\ A_{i\_(i+1)} &= \sqrt{t^2_{i\_(i+1)} + q^2_{i\_(i+1)}} \end{aligned} \tag{19}$$

applied by the panels.

It has been observed from the model array that the shaft rotates relative to panel $(i-1)\_i$ but remains stationary relative to panel $i\_(i+1)$. The same is true for all shafts and for both deployment and retraction. Therefore, a friction couple is applied to beam $(i-1)\_i$:

$$g_{1\_0} = -\mu s A_{0\_1}$$

$$g_{i\_(i-1)} = \pm\mu s\left(2T + A_{(i-1)\_i}\right) \qquad \begin{cases} + \text{ for } i = 2, 4, 6 \\ - \text{ for } i = 3, 5 \end{cases} \tag{20}$$

Note that, instead of calculating the resultant of the two forces transmitted between shaft and hinge, Eq. (20) simply considers the sum of their magnitudes. This assumption is made because the shafts are quite flexible and hence each force is transmitted directly to the nearest bearing.

The couple applied to the other side of the hinge and hence to beam $i\_(i+1)$ is calculated from equilibrium:

$$g_{1\_2} = \mu s(A_{0\_1} - D_1 - R_1)$$

$$g_{i\_(i+1)} = \mp\mu s\left(2T + A_{(i-1)\_i} - D_i - R_i\right) \qquad \begin{cases} - \text{ for } i = 2, 4, 6 \\ + \text{ for } i = 3, 5 \end{cases}$$

$$g_{7\_6} = 0 \tag{21}$$

Interaction with Gravity Compensation System

The preceding analytical model is purely two dimensional and hence does not consider any load components lying outside the x–y plane. Therefore, if its predictions are to be compared to the actual behavior of an array tested in a gravity environment, gravity effects should be canceled by applying to each hinge shaft a vertical force of constant magnitude, which is equal and opposite to the weight of that hinge assembly. However, in the experiments described earlier on the forces applied by the gravity cancellation system show a significant variation (Figs. 3d and 4d). Therefore, the analytical model has been modified to include, at each hinge, the additional in-plane forces induced by an out-of-plane bending moment, which is calculated, starting from the tip of the array, by considering the

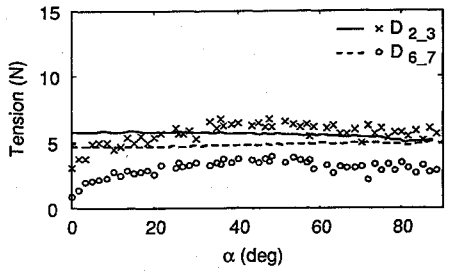

a) Deployment cable tensions

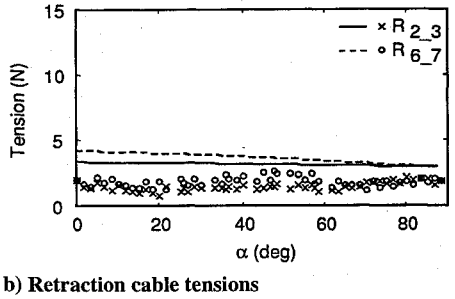

b) Retraction cable tensions

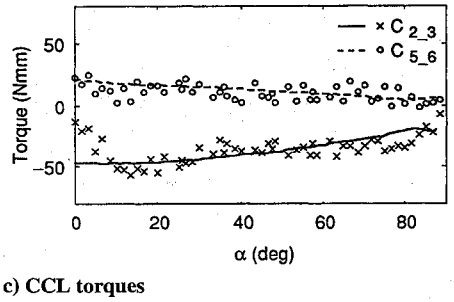

c) CCL torques

Fig. 9 Measured (×, ○) and predicted (continuous lines) deployment behavior.

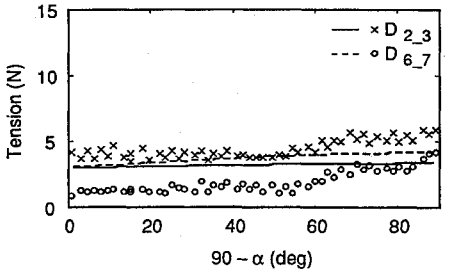

a) Deployment cable tensions

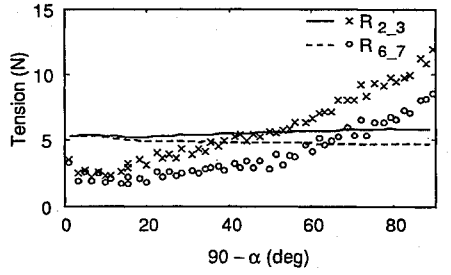

b) Retraction cable tensions

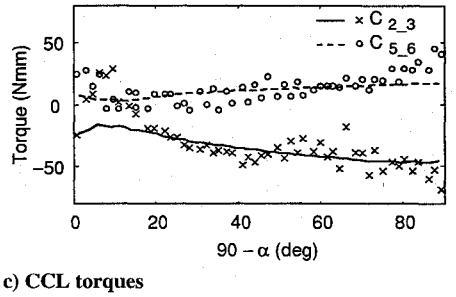

c) CCL torques

Fig. 10 Measured (×, ○) and predicted (continuous lines) retraction behavior.

difference between the weight of each hinge assembly and the force applied to that hinge by the gravity cancellation system.

Deployment/Retraction Predictions

The equilibrium equations set up in the preceding section have been solved iteratively for several values of α to simulate the deployment process. In each configuration, the equations are nonlinear because the load vector on the right-hand side depends on the values of the unknown internal variables; but only a few iterations are required to obtain convergence.

The deployment behavior of an array with the properties of the model array $L = 400$ mm, $\mu = 0.15$, $s = 3$ mm, and $p = 12.5$ mm has been simulated, both with and without inclusion of the interaction with the gravity compensation system. To include this interaction, the measured reactions from the support system, in the current configuration, are fed into the computations. It turns out that this interaction is not very significant because we are dealing with a small-scale, low-mass model. The inclusion of gravity effects introduces some noise in the deployment predictions and, overall, tends to improve the predictions by about 10%. The results of the simulation are plotted in Fig. 9 together with the measured behavior, replotted from Fig. 3.

The analytical model has been modified to simulate the retraction process by swapping the terms that correspond to the deployment and retraction cables in the equilibrium equations. The corresponding results are given in Fig. 10.

Discussion

Figure 9 shows that, excluding experimental noise, the analytical model is in excellent overall agreement with the deployment behavior of the model array and gives accurate predictions of the tension levels in all elements. The same general comments apply to the retraction behavior (see Fig. 10), but here the gradual increase of the tension in the retraction cable and the magnitude of the CCL torques have been somewhat underestimated.

The analytical model assumes that the motion is perfectly synchronized, and hence effects such as the initial tension buildup in the deployment cable and tension drop in the retraction cable, and the associated changes in CCL torques are not modeled. Similarly, the final prestressing of the hinges has not been modeled and, of course, inertia-related effects have been neglected.

Finally, the following two important features of cable-driven arrays have been noticed in the course of this study. First, it is essential that the $\boldsymbol{E}_i$ matrices, which appear in column 22 of the equilibrium matrix, should be as accurate as possible; although the angles between the deployment cable and the panels are small, they are not zero. This difference, if ignored, can lead to large inaccuracies and even singularity of the equilibrium matrix. Second, because of the low torsional stiffness of the panels, as the array deploys its overall bending stiffness changes considerably. Hence, it is difficult to adjust the gravity compensation system so that a uniform distribution of reactions will be maintained during deployment or retraction. The use of a softer support system is equally troublesome, and it is likely that an active system will be required for applications requiring optimal gravity compensation.

Acknowledgments

P. Kumar gratefully acknowledges financial support from the Cambridge Commonwealth Trust and the Nehru Trust. The authors are grateful to C. R. Calladine for helpful comments that have been incorporated in this revised version.

References

[1]Vorlicek, P. L., Gore, J. V., and Plescia, C. T., "Design and Analysis Considerations for Deployment Mechanisms in a Space Environment," NASA CP-2221, May 1982, pp. 211–222.

[2]Wie, B., Furumoto, N., Banerjee, A. K., and Barba, P. M., "Modeling and Simulation of Spacecraft Solar Array Deployment," *Journal of Guidance, Control, and Dynamics*, Vol. 9, No. 5, 1986, pp. 593–598.

[3]Nataraju, B. S., and Vidyasagar, A., "Deployment Dynamics of Accordion Type of Deployable Solar Arrays Considering Flexibility of Closed Control Loops," International Astronautical Federation, IAF Paper 87-256, Oct. 1987.

[4]Celli, J., Lomas, N., Pollard, H., and Totah, N., "Intelsat VII Solar Array Electrical and Mechanical Design," AIAA Paper 90-0780, March 1990.

[5]de Kam, J., "EURECA Application of the RARA Solar Array," *5th European Symposium Photovoltaic Generators in Space*, European Space Agency, Noordwijk, The Netherlands, 1986, pp. 105–114 (ESA-SP-267).

[6]Racca, G. D., Bongers, E., and Sebek, R., "Solar Array Mechanism Design and Performance," *EURECA Symposium*, European Space Agency, Noordwijk, The Netherlands, 1994, pp. 223–229.

[7]Kumar, P., and Pellegrino, S., "Deployment and Retraction of a Cable-Driven Solar Array: Testing and Simulation," NASA CP-3293, May 1995, pp. 253–267.

H. R. Anderson
Associate Editor